

# Self-Feeding Needleless Electrospinning of Cross-Linked Nanofibrous Materials for High-Performance Air Filtration

Han Li, Quangan Cai, Xiaoran Ming, Guilong Yan,\* Jingyu Chen, Zhenyu Li, Li Wang, Yuanpeng Wu, and Xungai Wang\*

Nanofibrous materials exhibit unique advantages in air filtration due to their high porosity, excellent pore connectivity, and large specific surface area. Electrospinning technology is the primary method for producing nanofibers. This study presents a novel needleless electrospinning system that features a unique self-feeding ability for polymer solution and generates fiber jets from a narrow self-feeding needleless, ensuring solution stability and high fiber productivity. This system combines the fiber quality advantage of traditional needle electrospinning with the high productivity of needleless electrospinning. In addition, by introducing melamine-formaldehyde (MF) as a crosslinking agent in the polyvinyl alcohol (PVA) polymer solution, the mechanical and waterproof properties of PVA nanofibers are improved. Experimental results indicate that the MF-PVA nanofibrous membrane exhibits excellent air filtration performance with high filtration efficiency (99.9%) and low air resistance (43 Pa), making it suitable for various applications such as face masks, protective clothing, and air filters.

H. Li, X. Wang

Joint Research Centre for Fiber Innovations and Renewable Materials (JRC-FIRM)

School of Fashion and Textiles

The Hong Kong Polytechnic University

Hung Hom, Kowloon, Hong Kong 999077, China

E-mail: xungai.wang@polyu.edu.hk

X. Ming, G. Yan, J. Chen, Z. Li, L. Wang, Y. Wu

 $The \, Center \, of \, Functional \, Materials \, for \, Working \, Fluids \, of \, Oil \, and \, Gas \, Field \, In \, Center \, of \, Functional \, Materials \, for \, Working \, Fluids \, of \, Oil \, and \, Gas \, Field \, In \, Center \, of \, Functional \, Materials \, for \, Working \, Fluids \, of \, Oil \, and \, Gas \, Field \, In \, Center \, of \, Functional \, Materials \, for \, Working \, Fluids \, of \, Oil \, and \, Gas \, Field \, In \, Center \, of \, Functional \, Materials \, for \, Working \, Fluids \, of \, Oil \, and \, Gas \, Field \, In \, Center \, of \, Functional \, Materials \, for \, Working \, Fluids \, of \, Oil \, and \, Gas \, Field \, In \, Center \, of \, Functional \, Materials \, for \, Working \, Fluids \, of \, Oil \, Center \, of \, Cente$ 

 ${\it School}\ of\ {\it New}\ Energy\ and\ Materials$ 

Southwest Petroleum University Chengdu 610500, China

E-mail: guilong.yan@swpu.edu.cn

Q. Cai

Key Laboratory of Advanced Technologies of Materials, School of Materials

Science and Engineering Southwest Jiaotong University

Chengdu 610031, China



The ORCID identification number(s) for the author(s) of this article can be found under https://doi.org/10.1002/smll.202505585

© 2025 The Author(s). Small published by Wiley-VCH GmbH. This is an open access article under the terms of the Creative Commons Attribution-NonCommercial License, which permits use, distribution and reproduction in any medium, provided the original work is properly cited and is not used for commercial purposes.

DOI: 10.1002/smll.202505585

# 1. Introduction

With the accelerated development of urbanization and industrialization, air pollution has become an increasingly severe environmental issue, posing significant threats to human health. In addition to common particulate matter, infectious diseases such as Coronavirus, Influenza A/B, and Mycoplasma pneumonia have also presented major challenges to public health and safety.[1-3] Traditional air filtration technologies often exhibit low filtration efficiency when dealing with particle sizes smaller than PM2,5. Nanofibrous materials have unique properties with high porosity, excellent pore connectivity, and large specific surface area, offering unique advantages in air filtration.[4,5] Electrospinning, the most widely used technology for the production of nanofibrous materials, allows precise control over the size, structure, and morphology of nanofibers. Electrospun nanofibrous

materials can effectively filter particles of specific sizes and have been applied in areas such as personal protection, filtration of dust and toxic substances, indoor air purification, and the filtration of viruses and bacteria in medical settings.<sup>[6-10]</sup>

Traditional electrospinning devices typically use single-needle setups, which have very low production efficiency and can only meet the needs of laboratory research. Since the demand for electrospun nanofibrous materials continues to grow, the challenge of scaling up electrospinning technology has become a critical issue that needs to be addressed urgently. Multi-needle electrospinning devices increase the number of Taylor cones by adding more needles, allowing for the adjustment of needle quantity to achieve industrial-scale production of nanofibers. Kim et al.[11] developed a novel cylindrical electrospinning system equipped with 120 needles, which produced smooth and bead-free polyurethane nanofibers with an average diameter of 230 nm. Although the spinning efficiency was significantly improved, the fiber morphology was difficult to control precisely due to the interference of electric fields among multiple needles. Akampumuza et al.[12] arranged six needles in triangular, square, and hexagonal layouts, demonstrating that the equilateral triangular pattern was the optimal multi-needle configuration for stable electrospinning. This layout effectively improved the uniformity of the electric field among the multiple jets and enhanced jet stability by reducing



www.advancedsciencenews.com

\_ SMQ

www.small-journal.com

charge repulsion. However, issues such as needle clogging and cleaning remain significant challenges.

The emergence of needleless electrospinning technology has provided new approaches for the industrial-scale production of electrospun nanofibers. The basic principle of needleless electrospinning is to utilize various spinneret structures to generate a large number of polymer droplets. When the applied high voltage exceeds the critical value, stable surface waves form on the free liquid surface of the polymer droplets. Jets are emitted from the wave peaks and eventually deposited onto the collector to form nanofibers. Niu et al.[13] conducted electrospinning experiments on polyvinyl alcohol and polyacrylonitrile solutions using round-edged cylinders, discs, and spheres as spinnerets. Ali et al.[14] employed a sprocket-shaped disc as the spinneret to produce nanofibers. This sprocket spinneret can initiate electrospinning at a relatively lower applied voltage and produce much finer nanofibers compared to a traditional disc spinneret. Wang et al.[15] discovered that nanofibers prepared using a helical coil spinneret exhibited a narrower diameter distribution. In this setup, the polymer solution was loaded onto the coil's surface through its slow rotation, with the viscoelasticity of the polymer solution contributing to the formation of a uniformly distributed solution layer on each spiral. When the applied voltage exceeded 40 kV, multiple jets were emitted from the coil's surface. However, prolonged exposure of the polymer solution to air caused solvent evaporation, which altered the concentration of the polymer solution over time. Wei et al.[16] introduced a needleless electrospinning spinneret based on a disc-shaped metal plate. The polymer solution was stored within the metal disc and was dispensed to the edge until a certain curvature was reached. The nanofibers produced by this metal disc spinneret had an average diameter of less than 240 nm with a narrowed diameter distribution, achieving both high-throughput production and uniform fiber diameters. However, the polymer solution needed to maintain a specific curvature range to initiate jet formation, making it difficult to achieve rapid, efficient, and continuous production. Elmarco's new Nano-Spider electrospinning device can produce nanofibers on an industrial scale via a stainless steel wire spinneret.[17] The device has the disadvantage that it requires a very high voltage, and due to solvent evaporation, a layer of polymer film will accumulate on the wire as the spinning time increases, which is difficult to clean.

Currently, research on needleless electrospinning primarily focuses on the optimized design of spinneret structures. However, there are still numerous challenges throughout the needleless electrospinning process, especially open systems. i) Changes in the concentration of the spinning solution due to solvent evaporation affect the distribution of fiber diameters. [18] ii) The accumulation of polymers on the electrode surface requires periodic cleaning, which limits the continuous production of nanofibers. iii) Mismatches in the liquid supply system affect the continuity of the spinning process.<sup>[19]</sup> iv) The preparation of spinning solutions often involves the use of large amounts of toxic and hazardous chemical reagents. During the jet solidification and fiber formation stages, the evaporation of solvents in large quantities can pose health risks to workers.<sup>[20]</sup> Therefore, developing green and efficient needleless electrospinning technology holds significant importance for the advancement of the nanofiber industry in the new era.

Herein, a novel enclosed needleless electrospinning setup was rationally designed to fabricate nanofibrous materials for air filtration. Compared to general needleless electrospinning with an open spinneret, this work generated fiber jets from a narrow edge, which ensures the stability of the solution and the fiber production output. Notably, no additional power was required to feed the polymer solution into the spinneret, owing to the effect of atmospheric pressure. There was no emission of toxic or hazardous chemicals during the electrospinning process since only water was used as the solvent. To improve the waterproof performance of polyvinyl alcohol (PVA) nanofibers, melamineformaldehyde (MF) was applied as the crosslinking agent. Moreover, MF-PVA nanofibrous membranes were tested with high filtration efficiency and low air resistance, showing great potential in numerous applications such as face masks, protective clothes, and air filters.

### 2. Results and Discussion

Generally, there is a trade-off between the nanofiber's quality and production rate. Nanofibers produced using traditional needlebased electrospinning have high quality but low production efficiency, while those produced by needleless electrospinning achieve high production rates but with lower quality. As a compromise, we developed a self-feeding needleless electrospinning system, which combines the advantages of needle-based and needleless electrospinning technologies. Unlike other needleless electrospinning, this system allows automatic solution feeding, inspired by the automatic water-feeding bottle on a farm (Figure 1a). The process is shown in Figure 1b. When the bottle in the water feeder is inverted into a water-filled tray with its mouth submerged below the water surface, the pressure generated by the water column inside the bottle is much less than the external atmospheric pressure. As the farm animals drink water from the tray and cause the water level in the tray to drop, the bottle's mouth will be exposed above the water surface. When this happens, air will enter the bottle through the mouth, increasing the pressure inside the bottle and causing the water inside the bottle to flow out. As the water level continues to drop, the water inside the bottle will keep flowing out until the bottle's mouth is submerged again, balancing the internal and external pressures, at which point the water flow stops. In this way, as long as there is water in the bottle, the water in the tray can be automatically replenished, achieving automatic water-feeding.

The self-feeding needleless electrospinning system is composed of a high-voltage power supply, rotary collector, self-supply box, wire spinneret, and stepper motor (Figure 1c). Once the applied voltage is over the critical value, nanofiber jets are generated from the spinneret and eventually deposited on the rotary collector. Meanwhile, the stepper motor allows a traversing and reciprocating motion to ensure the uniformity of the nanofibrous membrane over a set width. As shown in Figure 1d, the automatic feeding of polymer solution is fulfilled by the effect of the atmosphere. Since the polymer solution is sticky, the response time is longer than that of water. To enhance the response and jet initiation process, a thin wire is wrapped around the rod-shaped electrode. The finite element analysis result (Figure 1e; Figures S1 and S2, Supporting Information) revealed that the electric field is concentrated on the thin wire, which is beneficial for generating

16136829, 2025, 33, Downloaded from https://onlinelibrary.wiley.com/doi/10.1002/smll.202505585 by HONG KONG POLYTECHNIC UNIVERSITY HU NG HOM, Wiley Online Library on [05/10/2025]. See the Terms and Conditions

com/terms-and-conditions) on Wiley Online Library for rules of use; OA articles are governed by the applicable Creative Commons License

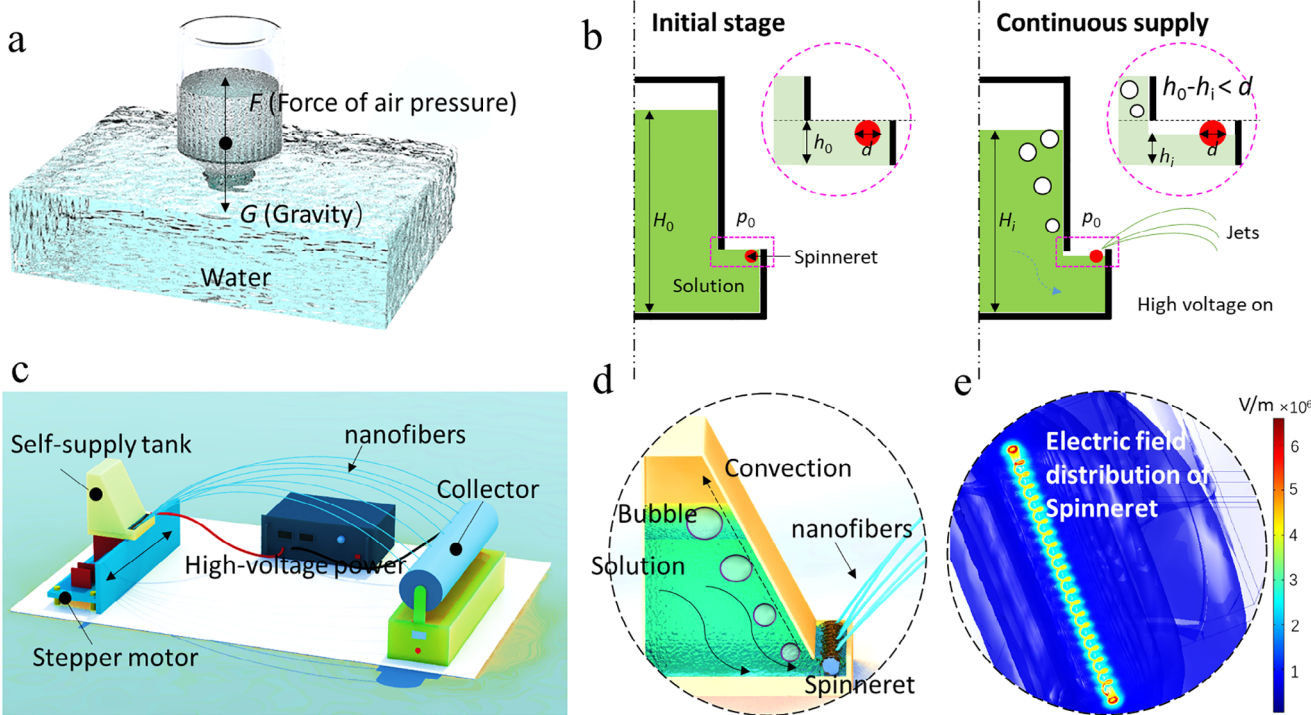


Figure 1. Illustration of self-feeding needleless electrospinning. a) Automatic water-feeding theory. b) Different stages of the automatic feeding system. c) 3D construction diagram of self-feeding needleless electrospinning system. d) Inner structure exhibition of the self-supply box via a cross-section view. e) Electric field distribution profile of the spinneret by finite element method.

nanofibrous jets. As the system is feeding automatically, the speed of generating nanofiber or productivity is determined by the electric field intensity. Numerous polymer jets were eventually deposited on the collector after the stretching and solidification process. The fiber diameter distribution was quite uniform, leading to the as-spun nanofibrous membrane with good quality (Figure S3, Supporting Information).

The formation mechanism of nanofibers by a self-feeding needleless electrospinning system is further studied. A digital charge couple device (CCD) camera was used to record the electrospinning process (Figure S4, Supporting Information). Unlike conventional needle electrospinning, all polymer jets were stretched into long and thin segments after the jet initiation process (Figure 2a). Dissipative particle dynamics (DPD) simulation results (Figure 2b) exhibited the whole process of nanofiber formation. The long stable stretch period may be attributed to the strong intermolecular force between water and MF-PVA, then unstable whipping due to the water evaporation (Figure 2c). To demonstrate the nanofiber formation process, polymer jets were captured at different distances from 10 to 25 cm. Scanning electron microscopy (SEM) results (Figure 2d) showed that nanofibers were still wet at 10 cm and dry when the distance increased to 25 cm. The average nanofiber diameter increased from 236 to 347 nm (Figure 2e), and the distribution became wider, which is consistent with the previous nanofiber formation hy-

PVA is a linear, semi-crystalline polymer composed of a carbon backbone as its main chain and hydroxyl functional groups as structural units. The existence of hydroxyl groups renders PVA a highly hydrophilic and water-soluble polymer. However, nanofibrous materials made solely from PVA often suffer from poor mechanical performance due to their high hydrophilicity, making them unstable in humid environments. [21] As a result, their functional properties tend to degrade during use. This work introduced melamine-formaldehyde (MF) as a crosslinking agent to improve their waterproof ability and strength.<sup>[22]</sup> As shown in Figure 3a, each melamine molecule has three amino groups, which can interact with more hydroxyl groups in the PVA main chains. Meanwhile, the molecular dynamics (MD) results showed that the cohesive energy density (CED) of the MF-PVA- $H_2O$  system (0.38 GJ m<sup>-3</sup>) is larger than that of the PVA- $H_2O$  system (0.27 GJ m<sup>-3</sup>), which means the MF-PVA-H<sub>2</sub>O system has a larger intermolecular force, leading to higher strength. With the increase in melamine concentration, the solution gradually became turbid (Figure 3b), which is attributed to the increased degree of crosslinking between melamine and PVA. For an open system, the solution is exposed to air, resulting in a large surface area for water evaporation, which leads to poor solution stability and affects the continuity of the spinning process. In contrast, for this system, the solution is sealed inside a container and is only exposed to air when the spinning process starts. As shown in Figure 3c, the setup ensures a stable fiber jet over a long period, which is beneficial for the continuity of the entire spinning process and meets the requirements of industrial production. Compared to open electrospinning (ES) systems (e.g., cylinder, coil, and ball spinneret), this self-feeding needleless electrospinning shows great advantages in solution stability (Figure 3d) and fiber diameter distribution (Figure 3e) for an 8-h workday. In

16136829, 2025, 33, Downloaded from https://onlinelibrary.wiley.com/doi/10.1002/smll.202505585 by HONG KONG POLYTECHNIC UNIVERSITY HU NG HOM, Wiley Online Library on [05/10/2025]. See the Terms

and Conditions (https://onlinelibrary.wiley.com/terms-and-conditions) on Wiley Online Library for rules of use; OA articles are governed by the applicable Creative Commons License

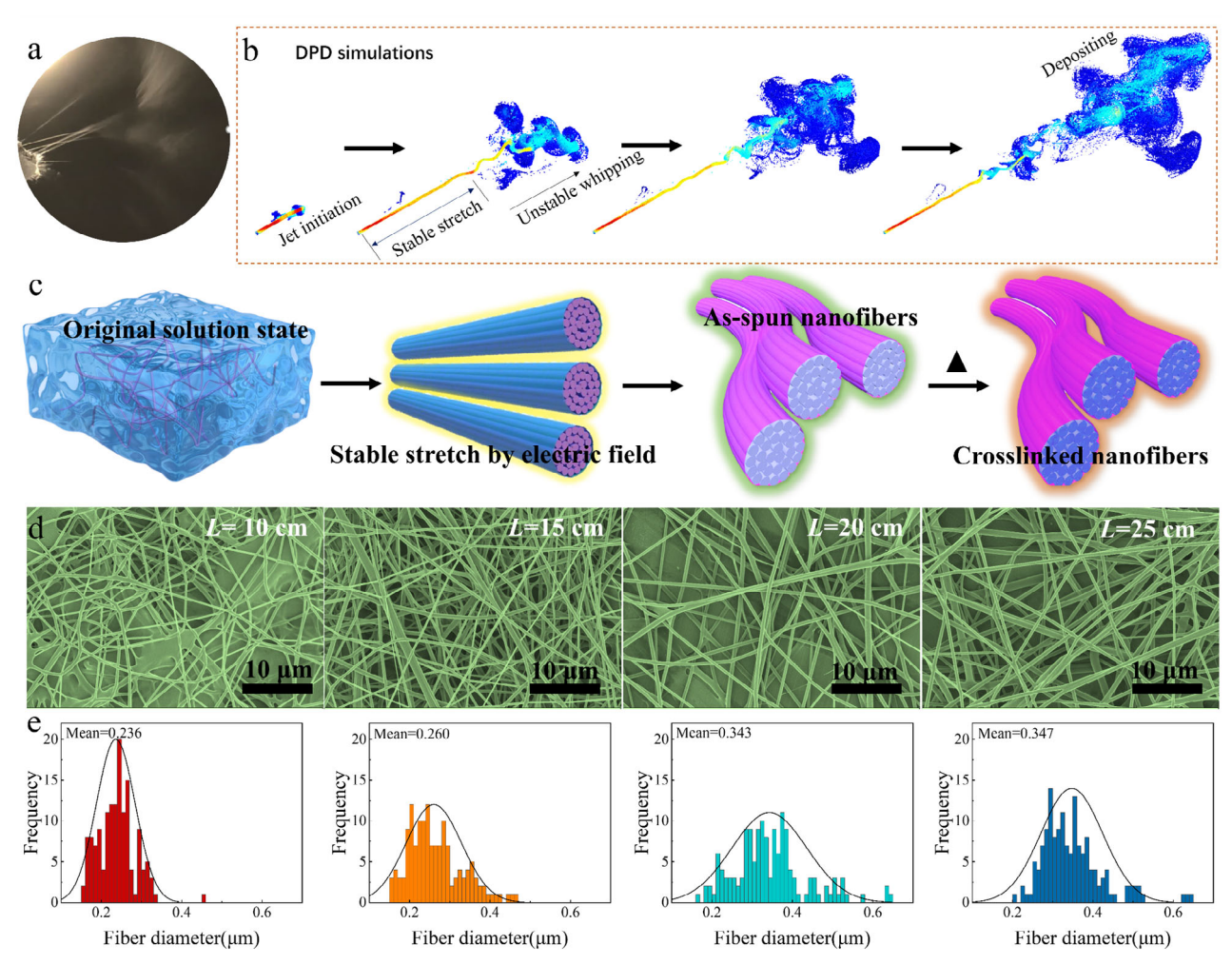


Figure 2. a) Self-feeding needleless electrospinning in action. b) DPD simulation results of nanofiber formation. c) Force analysis of polymer chains at different stages. d,e) SEM images and corresponding fiber diameter distribution diagrams of MF-PVA nanofibers fabricated by self-feeding needleless electrospinning at different collecting distances.

addition, the thermal-treated PVA nanofibers fabricated by open ES systems had low strength and many breakpoints.<sup>[23]</sup> While MF-crosslinked PVA nanofiber membrane showed excellent tensile properties and flawless appearance (Figure 3f; Figure S5, Supporting Information).

The air filtration performance of MF-PVA nanofibrous materials was further studied. The basis weight of nanofibers deposited on the collector can be controlled by adjusting the electrospinning time. **Figure 4a** shows MF-PVA nanofibrous filters with various transparencies. A larger basis weight leads to lower transparency and smaller pore size (Figure 4b). The filtration efficiency increased from 89.1% to 99.9% and the pressure drop increased from 38 to 136 Pa, when the basis weight increased from 0.23 to 0.68 g m<sup>-2</sup> (Figure 4c). This is due to the increase in fiber weight, which leads to a reduction in airflow channels, thereby intensifying the resistance to gas filtration. [24] The quality factor was introduced to evaluate the comprehensive performance of a filter. It can be calculated by the equation [25]

$$QF = -\ln(1-\eta)/\Delta P \tag{1}$$

where  $\eta$  is the filtration efficiency,  $\Delta P$  is the pressure drop. It is obvious that 0.34 g m<sup>-2</sup> of basis weight has the optimum quality factor of 0.0913 (Figure 4d). Compared to other commercial air filtration media, MF-PVA nanofibrous filters showed relatively low air resistance and high filtration efficiency (Figure 4e). The flow rate of the tested airflow also affects the air filtration performance. [26] The filtration efficiency decreased from 99.1% to 92.7%, and the pressure drop increased from 46 to 133 Pa, when the flow rate increased from 32 to 86 L min<sup>-1</sup> (Figure 4f).

To demonstrate the universality of the nanofibrous filters, outdoor filtration tests were carried on in Chengdu (Figure 5a). This city is located in the Sichuan Basin, surrounded by mountains and plateaus, creating a relatively enclosed environment that is not conducive to air circulation and the dispersion of pollutants. This geographical condition allows pollutants to accumulate locally, forming smog. In addition, Chengdu often experiences temperature inversions in winter, where a layer of warm air sits above cooler air near the ground. This stable atmospheric layer hinders the vertical dispersion of pollutants, causing them to accumulate near the surface. Climatic factors also play a significant

16136829, 2025, 33, Downloaded from https://onlinelibrary.wiley.com/doi/10.1002/smll.202505585 by HONG KONG POLYTECHNIC UNIVERSITY HU NG HOM, Wiley Online Library on [05/10/2025]. See the Terms

ditions) on Wiley Online Library for rules of use; OA articles are governed by the applicable Creative Commons Licenso

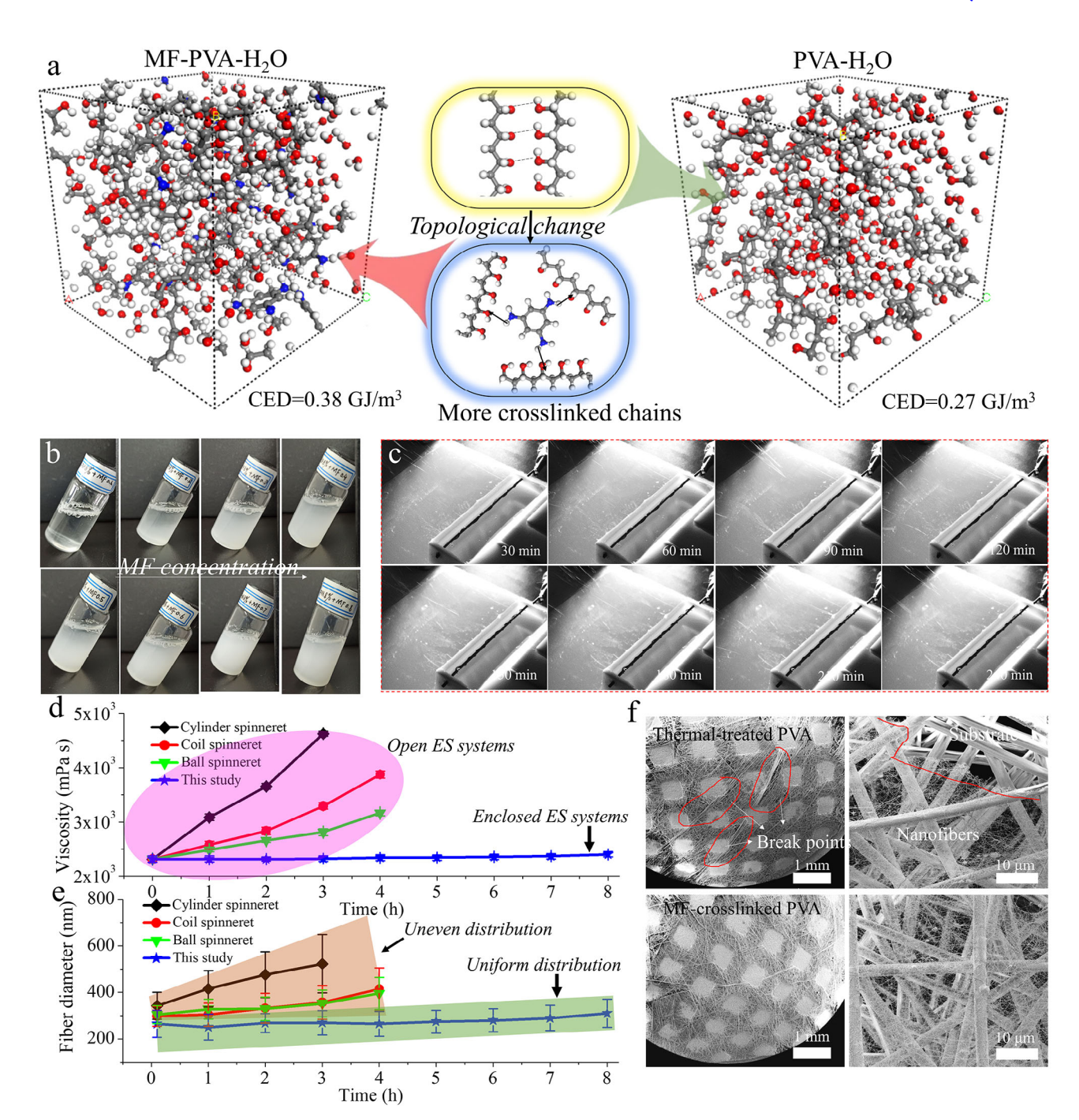


**Figure 3.** a) Molecular dynamics results of PVA-H<sub>2</sub>O and MF-PVA-H<sub>2</sub>O. b) Digital photographs of MF-PVA solutions with increased MF concentration. c) Video captions of self-feeding needleless electrospinning of MF-PVA solution. d) Comparison of solution viscosity between open ES systems and this study. e) Comparison of nanofiber diameters and distribution between the open ES system and this study. f) SEM images of thermal-treated PVA nanofibers by open ES system and MF-crosslinked PVA nanofibers by the self-feeding needleless electrospinning technology.

role in the formation of smog in Chengdu during winter. The wind speed is generally low, resulting in weakened atmospheric circulation and making it difficult for pollutants to disperse effectively. Moreover, the dry and less rainy climate conditions make it challenging for pollutants to be cleared by precipitation, further exacerbating the formation of smog. Figure 5a,b shows the results of the outdoor air filtration test from 2024/12/14 to

2025/01/14. Whether filtering PM<sub>2.5</sub> or PM<sub>10</sub> particles, the MF-PVA nanofibrous membrane has demonstrated excellent and stable filtration performance, showing great potential in home window screens, car dust filter bags, masks, and other applications.

SEM results (Figure 5c) showed that the morphology and fiber diameter had no changes after laundering. For thermal-treated PVA nanofibers, there is a noticeable decrease and

16136829, 2025, 33, Downloaded from https://olinelibrary.wiley.com/doi/10.1002/sml. 102025685 by HONG KONG POLYTECHNIC UNIVERSITY HU NG HOM, Wiley Online Library on (051002025). See the Terms and Conditions (https://olinelibrary.wiley.com/doi/10.1002/sml. 102025685 by HONG KONG POLYTECHNIC UNIVERSITY HU NG HOM, Wiley Online Library on (051002025). See the Terms and Conditions (https://olinelibrary.wiley.com/doi/10.1002/sml. 102025685 by HONG KONG POLYTECHNIC UNIVERSITY HU NG HOM, Wiley Online Library for rules of use.

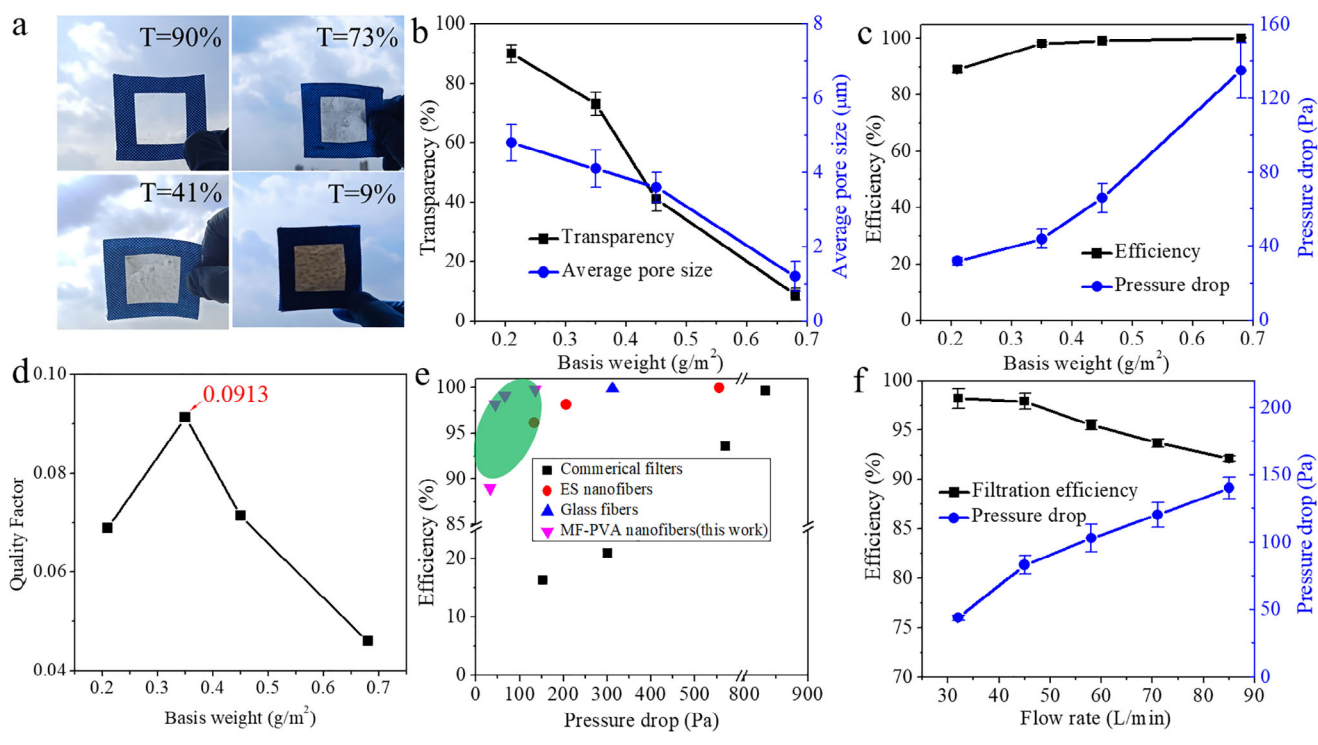


Figure 4. a) Digital images of air filters with different basis weights. b) Transparency and pore size varied with different basis weights. c) Filtration efficiency and pressure varied with different basis weights. d) Quality factor varied with different basis weights. e) Comparison of this nanofibrous filter with other commercial filters. f) Filtration efficiency and pressure varied with different flow rates.

unstable fluctuations in efficiency after laundering (Figure 5d), which was attributed to the low fiber membrane strength. [27,28] For MF-crosslinked PVA nanofibers, no significant change was observed in filtration efficiency (Figure 5e; Figure S6, Supporting Information). This is because the nanofibers maintained their intact morphology after laundering. Cycle filtration testing of polluted air was conducted by a self-made apparatus (Figure 5f). The MF-crosslinked PVA nanofibrous membrane product showed excellent stability in 3-h testing (Figure 5g). This is mainly due to the high mechanical and insoluble properties of the membrane.

# 3. Conclusion

In summary, the enclosed needleless electrospinning technology proposed in this study effectively addresses the challenges of low production efficiency and unstable fiber quality associated with traditional needle-based and needleless electrospinning methods, respectively. Through a novel automatic feeding system and the incorporation of MF as a crosslinking agent in the polymer solution, PVA nanofibers with significantly enhanced mechanical properties and waterproof capabilities were produced on a large scale. The MF-PVA nanofibrous membrane demonstrated exceptional air filtration performance with filtration efficiency reaching 99.9% and exhibited good stability under varying basis weights and flow conditions. This technology not only offers a new pathway for the industrial production of nanofibers but also contributes an effective material solution to combat air pollution, showcasing broad application prospects.

## 4. Experimental Section

<code>Materials: Polyvinyl alcohol (PVA, Mw = 146000-186000; 96% hydrolyzed) was purchased from J&K Chemical and used as received. Melamine-formaldehyde (AccuStandard, 50% in water) was used as a crosslinking agent. Deionized water was made by the laboratory setup and used as the solvent for dissolving PVA at 90  $^{\circ}$ C.</code>

Self-Feeding Needleless Electrospinning: The apparatus was composed of a self-supply box, a wire spinneret, a stepper motor, a power supply (ES100P, Gamma High Voltage Research) for charging the spinning solution, a rotary collector, as shown in Figure 1c. In this study, once the applied voltage is over the critical value, nanofiber jets are generated from the spinneret and eventually deposited on the rotary collector. Meanwhile, the stepper motor allowed a traversing and reciprocating motion to ensure uniform deposition of the nanofibrous membrane on a rotary collector over its width. In this study, the applied voltage was 25 kV, the PVA concentration was 9 wt.%, the MF concentration ranged from 0.2 to 1.0 wt.%, and the collecting distance was set at 25 cm away from the spinneret. Other details are shown in Table S1 (Supporting Information).

Characterizations: The morphology and structure of the fiber and membrane were observed by cold field emission scanning electron microscopy (FE-SEM) (Zeiss Supra 55, Germany). The fiber diameters were measured by Image J software based on SEM images. Porometer 3G specific surface area and pore diameter analyzer were used to test the size and distribution of the through-hole pore diameter of the fiber membrane. The transmittance measurement used a xenon lamp (150 W, Ocean Optics DH-2000-BAL) as the light source, coupled with a fast spectroradiometer (FLA 7200, Flight) to control the wavelength. The water immersion experiments were carried out by recording the weight change rate of the nanofibrous membrane absorbing water in 15 days.

Finite Element Analysis (FEA) of Airflow Field: The finite element analysis of the airflow field in the laminar flow model was carried out using

16136829, 2025, 33, Downloaded from https://online.library.wiley.com/doi/10.1002/smll.202505885 by HONG KONG POL YTECHNIC UNIVERSITY HU NG HOM, Wiley Online Library on [05/10/2025]. See the Terms and Conditions (https://onlinelibrary.wiley.com/doi/10.1002/smll.202505885 by HONG KONG POL YTECHNIC UNIVERSITY HU NG HOM, Wiley Online Library on [05/10/2025]. See the Terms and Conditions (https://onlinelibrary.wiley.com/doi/10.1002/smll.202505885 by HONG KONG POL YTECHNIC UNIVERSITY HU NG HOM, Wiley Online Library on [05/10/2025]. See the Terms and Conditions (https://onlinelibrary.wiley.com/doi/10.1002/smll.202505885 by HONG KONG POL YTECHNIC UNIVERSITY HU NG HOM, Wiley Online Library on [05/10/2025]. See the Terms and Conditions (https://onlinelibrary.wiley.com/doi/10.1002/smll.202505885 by HONG KONG POL YTECHNIC UNIVERSITY HU NG HOM, Wiley Online Library on [05/10/2025]. See the Terms and Conditions (https://onlinelibrary.wiley.com/doi/10.1002/smll.202505885 by HONG KONG POL YTECHNIC UNIVERSITY HU NG HOM, Wiley Online Library on [05/10/2025]. See the Terms and Conditions (https://onlinelibrary.wiley.com/doi/10.1002/smll.202505885 by HONG KONG POL YTECHNIC UNIVERSITY HU NG HOM, Wiley Online Library on [05/10/2025]. See the Terms and Conditions (https://onlinelibrary.wiley.com/doi/10.1002/smll.202505885 by HONG KONG POL YTECHNIC UNIVERSITY HU NG HOM, Wiley Online Library on [05/10/2025]. See the Terms and Conditions (https://onlinelibrary.wiley.com/doi/10.1002/smll.202505886 by HONG KONG POL YTECHNIC UNIVERSITY HU NG HOM, Wiley Online Library on [05/10/2025]. See the Terms and Conditions (https://onlinelibrary.wiley.com/doi/10.1002/smll.202505886 by HONG KONG POL YTECHNIC UNIVERSITY HU NG HOM, Wiley Online Library on [05/10/2025]. See the Terms and Conditions (https://onlinelibrary.wiley.com/doi/10.1002/smll.202505886 by HONG KONG POL YTECHNIC UNIVERSITY HU NG HOM POL YTECHNIC UNIV

onditions) on Wiley Online Library for rules of use; OA articles are governed by the applicable Creative Commons License

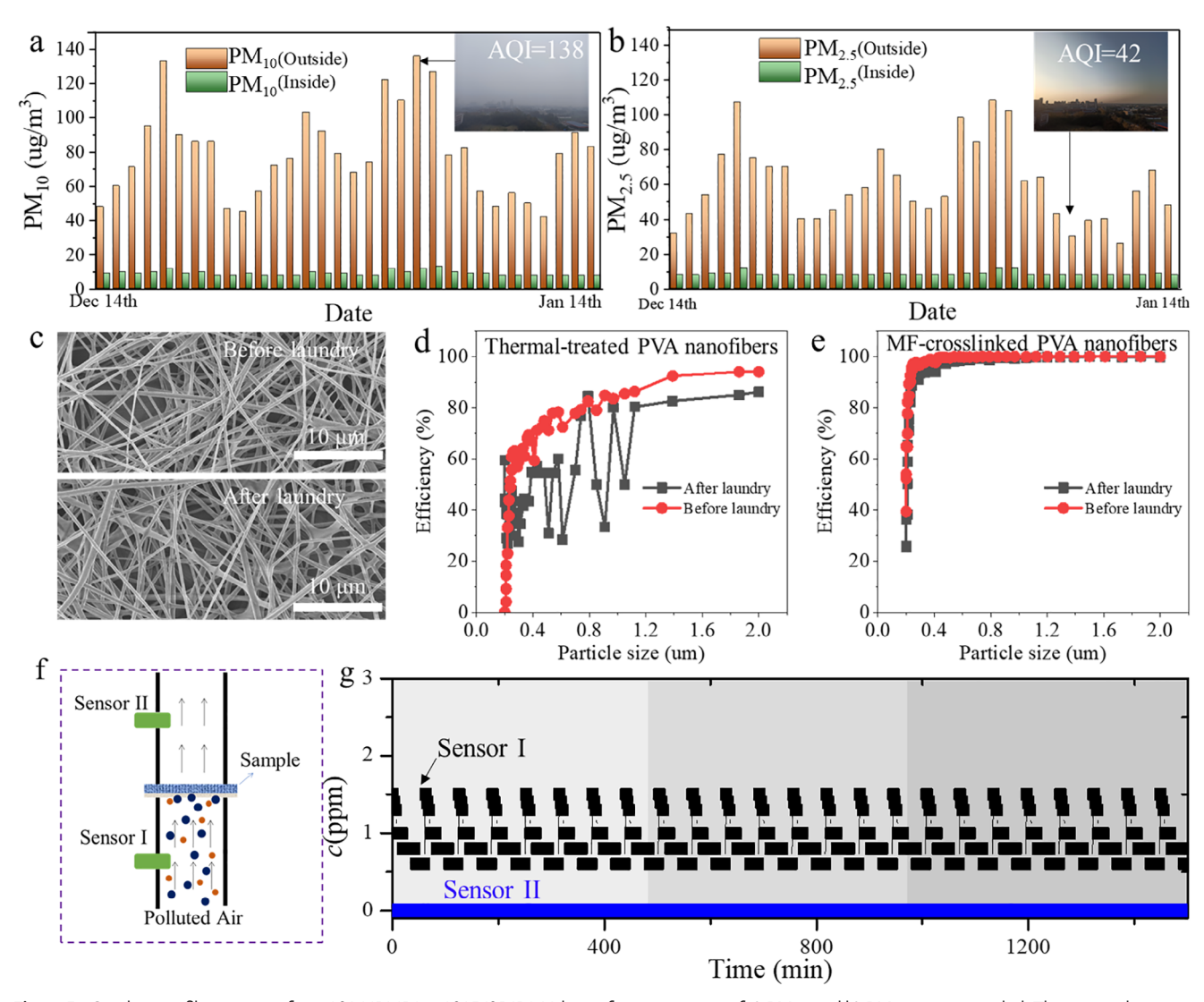


Figure 5. Outdoor air filtration test from 2024/12/14 to 2025/01/14. Values of concentration of a)  $PM_{10}$  and b)  $PM_{2.5}$  were recorded. The inserted pictures were the corresponding weather of Chengdu. c) SEM images of MF-crosslinked PVA nanofibers before and after laundering. d) Filtration efficiency of thermal-treated PVA nanofibers before and after laundry. e) Filtration efficiency of MF-crosslinked PVA nanofibers before and after laundry. f) Schematic of the filtration test for polluted air. g) Cycle filtration test of polluted air in 24 h.

COMSOL Multiphysics software. The geometric dimension was set to the actual size of the spinneret. The flow field was calculated according to the Navier-Stokes equation

$$\frac{\partial \nu}{\partial t} + \nu \cdot \nabla \nu = -\nabla p + \frac{\nabla^2 \nu}{Re} + f \tag{2}$$

where v is the air velocity, p is the air pressure and Re is the Reynolds number. The inlet airflow is set in the center of the slit, and the outlet is set as a collector, 25 cm away from the spinneret. In order to construct the grid of the airflow area, the maximum element size is set to 14.8 mm, and the minimum element size is set to 0.05 mm. The mesh size between the air plate and the spinneret is set to a maximum of 4 mm and a minimum of 0.008 mm. Other parameters have default settings.

Molecular Dynamic Simulation: For Molecular Dynamic (MD) Calculations, the PVA and MF-PVA chains were put into a periodic cell by the Amorphous Cell Construction of Materials Studio 8.0. The number of configurations was 100, and the density of the final configurations was 1

 $g^{\cdot}cm^{-3}$ . The forcefield type was the COMPASS and the system temperature was set as 298.0 K.

Filtration Test: The testing of the filtration performance of the samples is according to BS EN 1822–3:2009 standard. The test was carried out using the 8130 automatic filter performance tester (TSI Inc.), and the airflow was set as 32–86 L min $^{-1}$ . The aerosol used in the test is sodium chloride (NaCl) particles, with mass and quantity medium diameters of 260 and 75 nm, respectively. The airflow of the automatic filter material detector was set as 32 L min $^{-1}$ , and the sample area was  $10 \times 10 \text{ cm}^2$ , and the effective test area was  $100 \text{ cm}^2$ . The balanced relationship between filtration efficiency and filtration resistance is judged by introducing the quality factor (QF, PA $^{-1}$ ), as shown in the following

$$QF = -\ln(1 - \eta) / \Delta P \tag{3}$$

where  $\eta$  represents the filtration efficiency (%) of the material;  $\Delta$  P is the filtration resistance of the material (Pa).

16136829, 2025, 33, Downloaded from https://onlinelibrary.wiley.com/doi/10.1002/smll.202505885 by HONG KONG POLYTECHNIC UNIVERSITY HU NG HOM, Wiley Online Library on [05/10/2025]. See the Terms and Conditions (https://onlinelibrary.wiley.

conditions) on Wiley Online Library for rules of use; OA articles are governed by the applicable Creative Commons License

www.advancedsciencenews.com

# **Supporting Information**

Supporting Information is available from the Wiley Online Library or from the author.

# **Acknowledgements**

H.L. and Q.C. contributed equally to the work. The authors would like to acknowledge financial support by a grant from the Research Grants Council of the Hong Kong Special Administrative Region, China (Project No. PolyU 15209623) and the Sichuan Science and Technology Program (NO. 2023YFG0105).

### Conflict of Interest

The authors declare no conflict of interest.

# **Data Availability Statement**

The data that support the findings of this study are available from the corresponding author upon reasonable request.

## **Keywords**

air filtration, aqueous, nanofibrous membrane, needleless electrospinning

Received: May 8, 2025 Revised: June 11, 2025 Published online: June 18, 2025

- [1] H. Liu, S. C. Zhang, L. F. Liu, J. Y. Yu, B. Ding, Adv. Funct. Mater. 2019, 29, 1909554.
- [2] H. Liu, S. C. Zhang, L. F. Liu, J. Y. Yu, B. Ding, Adv. Funct. Mater. 2020, 30, 2000456.
- [3] C. A. Pope, Science 2019, 364, 536.
- [4] G. L. Yan, Z. H. Yang, H. Li, J. Y. Li, J. B. Wei, L. T. Shi, Z. Y. Li, J. Y. Chen, L. Wang, Y. P. Wu, Small 2022 19, 2206403.
- [5] Z. H. Yang, X. L. Zhang, Z. K. Qin, H. Li, J. Wang, G. Y. Zeng, C. H. Liu, J. P. Long, Y. X. Zhao, Y. F. Li, G. L. Yan, Small 2022, 18, 2107250.

- [6] S. C. Zhang, H. Liu, N. Tang, S. Zhou, J. Y. Yu, B. Ding, Adv. Mater. 2020, 32, 2001457.
- [7] R. L. Sun, G. L. Yan, X. L. Zhang, Z. Y. Li, J. Y. Chen, L. Wang, Y. P. Wu, Y. Q. Wang, H. Li, Chem. Eng. J. 2023, 455, 430.
- [8] G. L. Yan, Z. H. Yang, X. L. Zhang, H. Li, L. Wang, Z. Y. Li, J. Y. Chen, Y. P. Wu, Chem. Eng. J. 2023, 461, 142137.
- [9] H. Li, H. Y. Zhao, G. L. Yan, G. Y. Huang, C. Ge, M. Forsyth, P. C. Howlett, X. A. Wang, J. Fang, Small 2023, 20, 2304844.
- [10] H. Li, G. L. Yan, H. Y. Zhao, P. C. Howlett, X. A. Wang, J. Fang, Adv. Mater. 2024, 36, 2311272.
- [11] I. G. Kim, J. H. Lee, A. R. Unnithan, C. H. Park, C. S. Kim, J. Ind. Eng. Chem. 2015, 31, 251.
- [12] O. Akampumuza, H. C. Gao, H. N. Zhang, D. Q. Wu, X. H. Qin, Macromol. Mater. Eng. 2018, 303, 3395.
- [13] H. T. Niu, X. G. Wang, T. Lin, J. Text. Inst. 2012, 103, 787.
- [14] U. Ali, H. T. Niu, S. Aslam, A. Jabbar, A. W. Rajput, T. Lin, J. Mater. Sci. 2017. 52. 7567.
- [15] X. Wang, H. T. Niu, X. G. Wang, T. Lin, J. Nanomater. 2012, 2012, 785920.
- [16] L. Wei, R. J. Sun, C. K. Liu, J. Xiong, X. H. Qin, Mater. Des. 2019, 179, 107577.
- [17] M. Yu, R.-H. Dong, X. Yan, G.-F. Yu, M.-H. You, X. Ning, Y.-Z. Long, Macromol. Mater. Eng. 2017, 302, 1700002.
- [18] G. Zheng, Z. Gui, Q. Wang, R. Chen, R. Shen, S. Guo, H. Yan, Y. Liu, Z. Shao, J. Clean Prod. 2025, 486, 144562.
- [19] Z. Shao, Q. Wang, Z. Gui, R. Shen, R. Chen, Y. Liu, G. Zheng, Sep. Purif. Technol. 2025, 358, 130417.
- [20] E. S. Mousavi, N. Kananizadeh, R. A. Martinello, J. D. Sherman, Environ. Sci. Technol. 2021, 55, 4134.
- [21] Y. Deng, M. Zhu, T. Lu, Q. Fan, W. Ma, X. Zhang, L. Chen, H. Min, R. Xiong, C. Huang, Sep. Purif. Technol. 2023, 304, 122235.
- [22] J. Cui, Y. Wang, T. Lu, K. Liu, C. Huang, J. Colloid Interf. Sci. 2021, 597,
- [23] Y. Deng, T. Lu, J. Cui, W. Ma, Q. Qu, X. Zhang, Y. Zhang, M. Zhu, R.
- Xiong, C. Huang, Sep. Purif. Technol. 2022, 294, 121093. [24] Z. Fu, T. Zhao, H. Wang, J. Wei, H. Liu, L. Duan, Y. Wang, R. Yan, J.
- Bioresour. Bioprod. 2024, 9, 351.
- [25] S. Zhang, H. Liu, N. Tang, S. Zhou, J. Yu, B. Li, B. Ding, Adv. Mater. **2020**, 32, 2006930.
- [26] Y. Deng, T. Lu, X. Zhang, Z. Zeng, R. Tao, Q. Qu, Y. Zhang, M. Zhu, R. Xiong, C. Huang, J. Membrane Sci. 2022, 660, 120857.
- [27] C. Cai, Y. Sun, Y. Chen, Z. Wei, Y. Wang, F. Chen, W. Cai, J. Ji, Y. Ji, Y. Fu, J. Bioresour. Bioprod. 2023, 8, 421.
- [28] Y. Zhao, Z. Yang, R. Zhou, B. Zheng, M. Chen, F. Liu, W. Miao, R. Zhou, P. Cullen, Z. Xia, L. Dai, K. Ostrikov, J. Bioresour. Bioprod. 2024, 9, 369.